Gate-Opening Gas Adsorption and Host−Guest Interacting Gas Trapping Behavior of Porous Coordination Polymers under Applied AC Electric Fields

Wataru Kosaka,[†,‡] Kayo Yamagishi,[§] Jun Zhang,[‡] and Hitoshi Miyasaka*,[†,‡]

[†]Institute for Materials Research, Tohoku University, 2-1-1 Katahira, Aoba-ku, Sendai 980-8577, Japan
[‡]Department of Chemistry, Graduate School of Science, Tohoku University, Aramaki-Aza-Aoba, Aoba-ku, Sendai 980-8578, Japan
[§]Department of Chemistry, Division of Material Sciences, Graduate School of Natural Science and Technology, Kanazawa University, Kakuma-machi, Kanazawa 920-1192, Japan

S *Supporting Information*

ABSTRACT: The gate-opening adsorption behavior of the one-dimensional chain compound $[Ru_2(4\text{-}Cl\text{-}2\text{-}OMePh\text{-}CO_2)_4(phz)]$ (**1**; $4\text{-}Cl\text{-}2\text{-}OMePhCO_2^-$ = 4-chloro-*o*-anisate; phz = phenazine) for various gases (O_2, NO, and CO_2) was electronically monitored *in situ* by applying ac electric fields to pelletized samples attached to a cryostat, which was used to accurately control the temperature and gas pressure. The gate-opening and -closing transitions induced by gas adsorption/desorption, respectively, were accurately monitored by a sudden change in the real part of permittivity (ε'). The transition temperature (T_{GO}) was also found to be dependent

on the applied temperature and gas pressure according to the Clausius−Clapeyron equation. This behavior was also observed in the isostructural compound $[Rh_2(4\text{-}Cl\text{-}2\text{-}OMePhCO_2)_4(phz)]$ (**2**), which exhibited similar gate-opening adsorption properties, but was not detected in the nonporous gate-inactive compound $[Ru_2(o\text{-}OMePhCO_2)_4(phz)]$ (**3**). Furthermore, the imaginary part of permittivity (ε'') effectively captured the electronic perturbations of the samples induced by the introduced guest molecules. Only the introduction of NO resulted in the increase of the sample's electronic conductivity for **1** and **3**, but not for **2**. This behavior indicates that electronic host−guest interactions were present, albeit very weak, at the surface of sample **1** and **3**, i.e., through grain boundaries of the sample, which resulted in perturbation of the conduction band of this material's framework. This technique involving the *in situ* application of ac electric fields is useful not only for rapidly monitoring gas sorption responses accompanied by gate-opening/-closing structural transitions but also potentially for the development of molecular framework materials as chemically driven electronic devices.
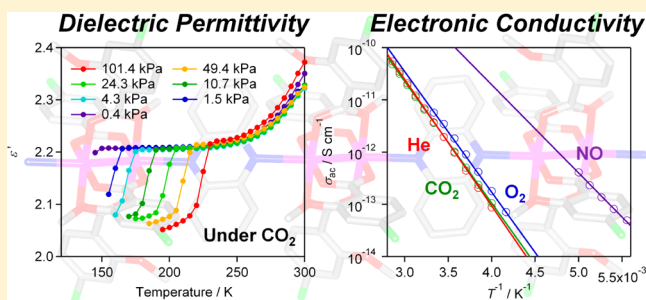
■ INTRODUCTION

In recent years, molecular porous materials, referred to as porous coordination polymers (PCPs)[1] or metal−organic frameworks (MOFs),[2] have attracted much attention as selective gas adsorption materials.[3] Selective gas adsorption is largely achieved by creating host−guest interactions[4] and/or guest-induced gate-opening structural transformations that only occur in the presence of a specific gas molecule.[5] Technically, in general, the gas adsorption process can be observed by monitoring the equilibrium gas pressure versus a known applied pressure for a significant sample weight; however, a large sample size is required and the time to achieve equilibrium, which is dependent on the nature of the material, can be extensive. Furthermore, this method does not provide any direct information on the dynamic properties of the adsorption process or the electronic interactions between host frameworks and guest molecules, although abrupt adsorptions or hysteresis gas adsorption/desorption processes, which may be an indication of gate-opening behavior or host−guest

interactions, are recognizable from the gas sorption isotherms. So, how can the occurrence of gas adsorption accompanied by gate-opening transitions be detected without affecting the sorption isotherms? In addition, how can *in situ* analysis of chemical host−guest interactions be achieved during gas adsorption? Other specific techniques except directly taking an adsorption isotherm were also useful for getting information on materials or guest molecules in the adsorption process; for example, the following techniques were available: nuclear magnetic resonance (NMR for several probes such as ^{13}C,[6] ^{19}F,[7] ^{129}Xe[8]), infrared spectroscopy (IR),[9,10] Raman spectroscopy,[11] fluorescence spectroscopy,[12] UV−vis spectroscopy,[13] impedance spectroscopy (for proton conduction in pores),[14] magnetic measurements,[15] differential scanning calorimetry (DSC),[16] inelastic neutron scattering (INS for the H_2 adsorption),[9h,17] neutron powder diffraction (NPD for the D_2

adsorption),[18] near-edge X-ray absorption fine structure spectroscopy (NEXAFS),[19] X-ray powder diffraction (XRPD),[4f,9m,n,q,10,12a,20] and single-crystal X-ray diffraction analysis.[16a,21]

Herein, we propose the utility of *in situ* ac electric field measurements not only for accurately monitoring such gate-opening gas adsorption properties of PCPs/MOFs but also for understanding the electronic effect due to the host−guest electronic interaction. The gate-opening structural transition enables a transient dielectric response even in a transformation between symmetrical unit cells for adsorbed/desorbed forms. For electronically conjugated polymers that are potentially good electronic conductors, this technique sensitively detects even very small electronic changes when guest molecules are introduced and electronically perturb the framework of the material. In other words, the physical properties of a framework can possibly be tuned by the introduction of specific gas molecules, which could potentially enable the creation of novel molecular systems/sensors driven by chemical information as an external stimulus. For such a strategy, specific MOFs/PCPs, which are redox-active vs a guest molecule and electronically conjugated through the framework, are required to be designed, even though general MOFs/PCPs reported previously have been insulators.

Recently, we reported selective nitric oxide (NO) adsorption accompanied by gate-opening structural changes in the one-dimensional chain compound $[Ru_2(4\text{-}Cl\text{-}2\text{-}OMePh\text{-}CO_2)_4(phz)]$ (**1**, 4-Cl-2-OMePhCO$_2^-$ = 4-chloro-*o*-anisate; phz = phenazine) (Figure 1), which was synthesized from an electronically activated (i.e., having a highly donating character) paddlewheel-type carboxylate-bridged diruthenium(II, II) unit (hereafter denoted as $[Ru_2]$)[22,23] linked by phenazine.[10] While

the sorption isotherms for O_2 and CO_2 exhibited simple monotonic adsorption/desorption features with the first gate-opening transitions, the sorption isotherm for NO showed an adsorption/desorption hysteresis phenomenon involving a two-step gate-opening transition during the adsorption process (inset of Figure S1).[10] The *in situ* infrared spectroscopy analysis revealed the existence of interacting NO molecules that are likely in the charge distributed state $D^{\delta+}\cdots(NO)^{\delta-}$ (D = the $[Ru_2]$-phz framework) (Figure 1). An isostructural compound with a paddlewheel $[Rh_2]$ analogue (**2**; Figure 1), which was almost redox-inert, also exhibited specificity toward NO adsorption, but not to the same extent as **1**. In this study, ac electric fields were applied to these materials during gas adsorption, and changes in the electrical properties were measured *in situ*, including: (i) the dielectric response, which indicates gate-opening phenomena for gas adsorption/desorption and (ii) the electronic effects of interaction with a specific introduced gas (i.e., NO). To further characterize these effects, the nonporous $[Ru_2]$-phz chain compound $[Ru_2(o\text{-}OMePhCO_2)_4(phz)]$ (**3**), with a similar degree of donating ability as that of **1**, was used as a reference (Figure 1). Ac electric field measurements were clearly demonstrated to be extremely useful for the highly sensitive detection of electric output signals in response to gas adsorption involving the gate-opening process and/or chemical interactions between the framework and guest molecules.

■ RESULTS AND DISCUSSION

Characterization of Nonporous [Ru₂]-phz Chain (3) as a Reference. In the course of a recent study of a series of anisate-bridged $[Ru_2]$ compounds with phz linkages,[10] the one-dimensional chain compound $[Ru_2^{II,II}(o\text{-}OMePhCO_2)_4(phz)]$ (**3**) was obtained. The original anisate-bridged $[Ru_2]$ unit $[Ru_2^{II,II}(o\text{-}OMePhCO_2)_4(THF)_2]$ possesses a high electron-donating character as indicated by its redox potential of −228 mV (vs Ag/Ag$^+$ in THF), while the similar compound $[Ru_2^{II,II}(4\text{-}Cl\text{-}2\text{-}OMePhCO_2)_4(THF)_2]$ has a redox potential of −131 mV. In the corresponding chain compounds, the THF molecules that axially cap the $[Ru_2]$ units in these systems are substituted by phz.[10] The chain form of compound **3** is similar to that of **1** and **2**, but this nonporous material crystallizes without an inner crystallization solvent in the triclinic $P\overline{1}$ space group (Table S1).

Notably, one-half of the formula unit, with inversion centers at the midpoint of the Ru−Ru bond and the center of the phz molecule, was determined to be an asymmetric unit (Z = 1) (Figure 2a; selected bond distances and angles are given in Table S2). The oxidation state of the $[Ru_2]$ unit in **3** was assigned as $[Ru_2^{II,II}]$, as in the case for **1**, and was confirmed by the local dimensions of its structure (see Table S2 and the related description in the Supporting Information) and its magnetic properties (Figure S2). Chains with a $[-(Ru_2)-phz-]$ repeating unit run along the *a* axis (Figure 2b,c) with no specific interactions (e.g., $\pi-\pi$ interactions) between neighboring chains. In addition, the void space around the chains is minimal at 26.8 Å^{3},[24] which corresponds to 2.7% of the total volume. The nonporous nature of **3** was confirmed on the basis of the gas adsorption measurement results; gas uptake was not observed below 100 kPa for N_2 at 77 K, CO_2 at 195 K, O_2 at 90 K, or NO at 121 K (Figure S1). Thus, the gate-opening behavior for gas adsorption was not induced in **3**, even when characteristic interchain interactions, such as $\pi-\pi$ and CH$\cdots\pi$ interactions, were not detected.
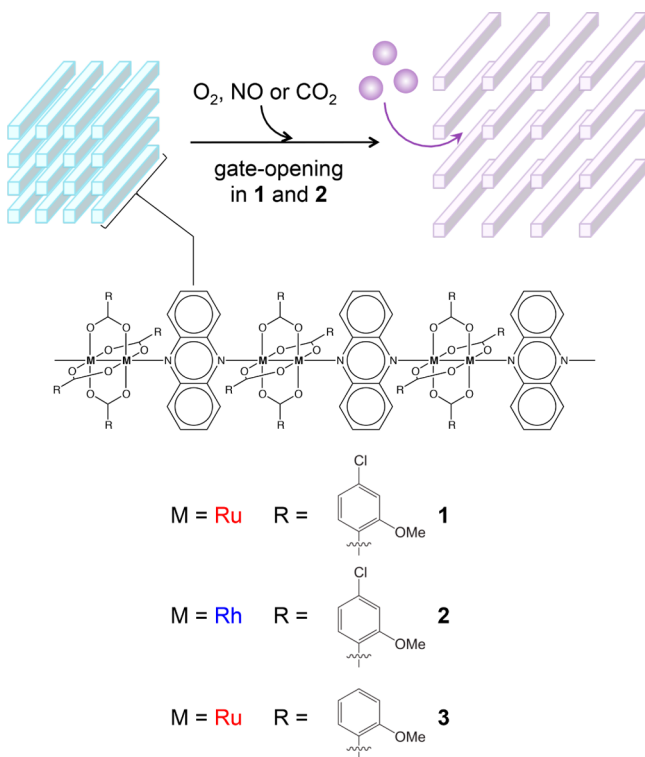
Figure 1. Schematic of the one-dimensional chain compounds $[M_2^{II,II}(RCO_2)_4(phz)]$ and an image of the gate-opening structural transition induced by inserted gas molecules.

a)

b)

c)
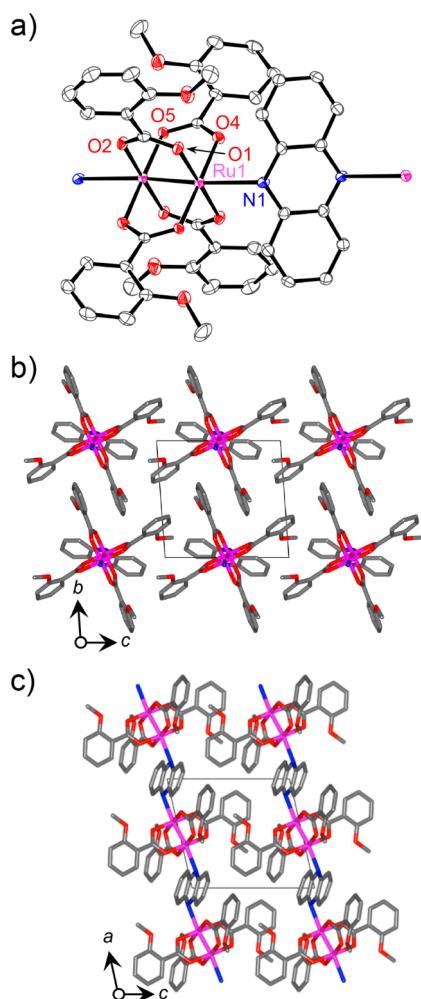
Figure 2. Structure of **3**: thermal ellipsoid plot (50% probability level) of the asymmetric unit with atom numbering schemes (a) and packing views projected along the *a* axis (b) and the *b* axis (c), where atoms O, C, N, and Ru are represented in red, gray, blue, and purple, respectively. Hydrogen atoms are omitted for clarity.

***In situ* Dielectric Measurements.** In many cases, gas adsorption properties have been investigated at temperatures just above the boiling points of the employed gases used because the thermal activation of the gas molecules introduced to the pores should be suppressed as much as possible to achieve close-contact packing. However, the quantity of gas introduced into the pores should strongly be dependent on the temperature and gas pressure[25] according to the Clausius–Clapeyron equation: $dP/dT = L/T\Delta\upsilon$, where *L* is the specific latent heat (i.e., the adsorption enthalpy) and $\Delta\upsilon$ is the specific volume change due to the transition (i.e., the volume change between the gas and condensed phases in the pores).[16,25,26] When a gate-opening transition is involved, however, *L* should be replaced by the transition enthalpy for gate-opening, H_{Trans}: $dP/dT = H_{Trans}/T\Delta\upsilon$. Hence, measurement of permittivity $(\varepsilon(\omega) = \varepsilon'(\omega) + i\varepsilon''(\omega)$; ε' = the real part; ε'' = the imaginary part; ω = the angular frequency $(\omega = 2\pi\nu))$ as a function of temperature is sensible for understanding the nature of the gate-opening process and the electron transport properties of the framework induced by the introduction of the gas. Therefore, pellet samples prepared from ground powders of **1–3** were sandwiched between electrodes comprising stainless plates with a diameter of 10 mm ϕ that were attached to Au

wires, and these electrode sets were then placed in a cryocell for which the gas pressure could be accurately controlled (see the Experimental Section).

Accurate Detection of Gate-Opening Adsorptions via Analysis of $\varepsilon'-T$ Plots. The temperature dependence of the permittivities of **1–3** was measured at ac electric field frequencies of 0.1, 1, and 10 kHz under a gas pressure of 100 kPa. Figure 3 shows the relative permittivity variation for **1**
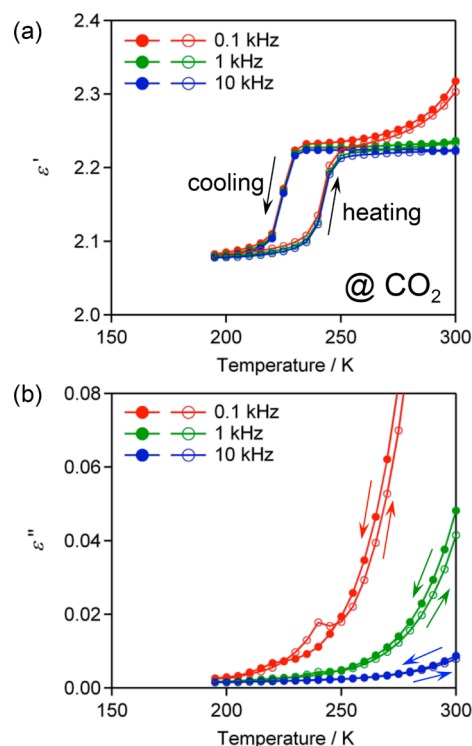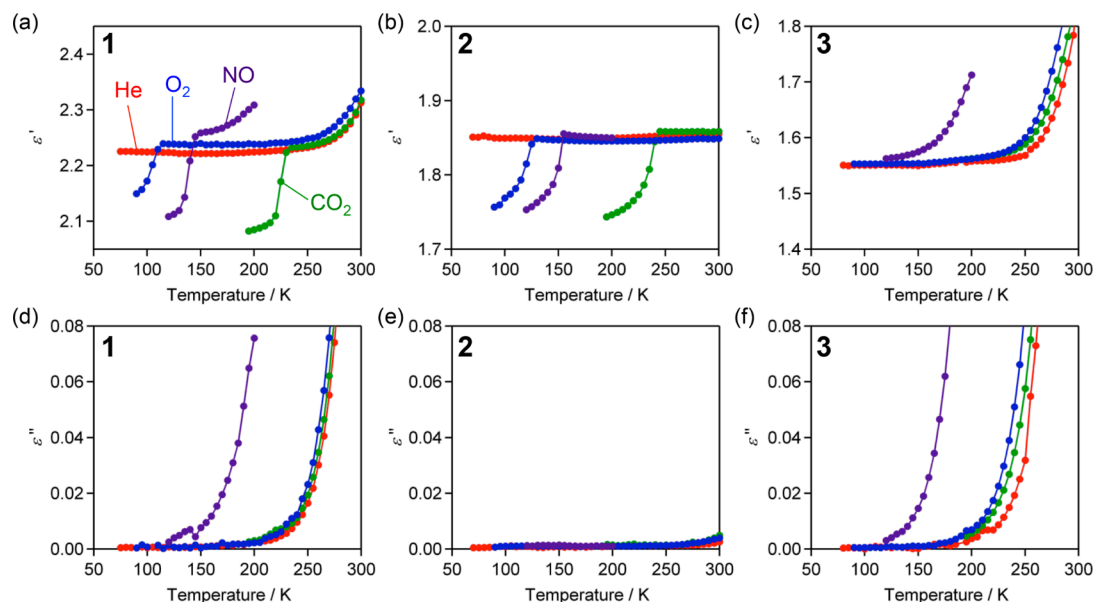

Figure 3. Temperature dependence of the (a) real part (ε') and (b) imaginary part (ε'') of the dielectric constant for **1** measured during cooling (closed circles) and heating (open circles) under 100 kPa of CO_2 with ac electric field frequencies ranging from 0.1 to 10 kHz.

during cooling and heating under a CO_2 atmosphere. During cooling, an abrupt decrease in the ε' value corresponding to approximately a −7% change was observed at 231 K in a frequency-independent manner, indicating that CO_2 adsorption suddenly occurred at this temperature; in other words, the gates of the pores for gas accommodation were opened at this temperature at a CO_2 pressure of 100 kPa. Thus, 231 K is the gate-opening structural transition temperature $T_{GO\downarrow}$(100 kPa of CO_2) for these conditions; Table 1 summarizes gate-opening

Table 1. Gate-Opening ($T_{GO\downarrow}$) and -Closing ($T_{GO\uparrow}$) Temperatures for 1 and 2 under 100 kPa of CO_2, NO, and O_2, Where $\Delta T_{GO} = T_{GO\uparrow} - T_{GO\downarrow}$

compounds		CO_2	NO	O_2
	$T_{GO\downarrow}$ (K)[a]	231	143	112
1	$T_{GO\uparrow}$ (K)[a]	247	161	121
	ΔT_{GO} (K)	16	18	9
	$T_{GO\downarrow}$ (K)[a]	242	155	127
2	$T_{GO\uparrow}$ (K)[a]	252	160	132
	ΔT_{GO} (K)	10	5	5

[a]$T_{GO\downarrow}$ and $T_{GO\uparrow}$ were defined as the points at which the value was leaved from and returned to the normal value, respectively.
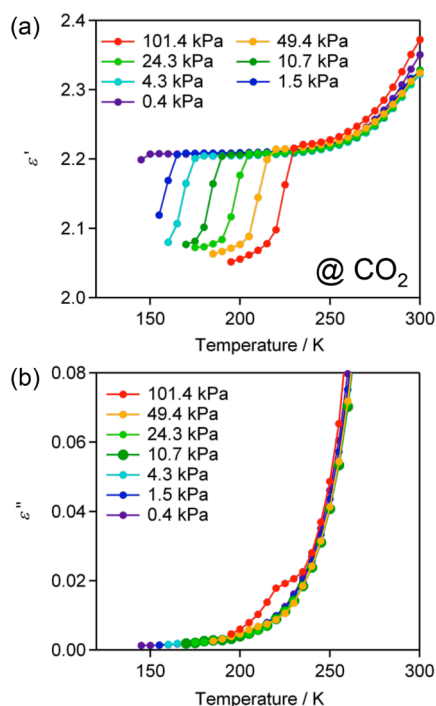
Figure 4. Temperature dependence of the dielectric constants for **1** (a) and (d), **2** (b) and (e), and **3** (c) and (f) measured during cooling with an applied electric field frequency of 0.1 kHz under 100 KPa of He (red), CO_2 (green), O_2 (blue), and NO (violet): (a)−(c) real part (ε') and (d)−(f) imaginary part (ε'').

($T_{GO\downarrow}$) and -closing ($T_{GO\uparrow}$) temperatures for **1** and **2** under 100 kPa of CO_2, together with those of NO and O_2 (vide infra). During heating (from 195 K), the ε' value steeply increased at approximately 240 K and recovered at 247 K, indicating the gate-closing structural transition temperature $T_{GO\uparrow}$(100 kPa of CO_2) $\approx$ 247 K (here, the transition temperature was defined as the point at which the value returned to normal). Thus, the gate-opening and -closing behaviors at a given gas pressure were detectable as a clear change in the value of ε' as a function of the temperature, and for this system, thermal hysteresis (ΔT_{GO}) with a temperature width of ca. 15 K was observed (Table 1). Note that the value of ε' at temperatures above T_{GO} was frequency-dependent and increased with temperature; ε' values at 0.1 kHz were larger than those at 10 kHz. This behavior is likely due to the influence of currents leaking through the grain boundaries of the sample. Indeed, a frequency-dependent monotonic increase in the value of ε'' was observed as the temperature increased, indicating that compound **1** itself exhibits limited electronic conductivity, which can be realized from the temperature-dependent behavior of $\varepsilon'' \propto 1/\omega R$ (R = resistance), as described in detail in the following section.[27]

In addition to the response for **1** observed under a CO_2 pressure of 100 kPa, a drastic change in the value of ε' was detected for NO and O_2, but not for He ($T > 70$ K), as can be seen in Figure 4a, for $\nu = 0.1$ kHz during cooling (the behavior at other frequencies was similar to that under CO_2; see Figure 3). The gate-opening temperatures for **1** under NO and O_2 with $P = 100$ kPa ($T_{GO\downarrow}$(100 kPa)) were 143 and 112 K, respectively (Table 1). These temperatures are approximately correlated to the critical temperatures T_c of these gases (T_c = 304 K for CO_2, 180 K for NO, and 155 K for O_2). Most importantly, the change in the value of ε' definitely provided an indication of gate-opening adsorption at a given pressure of gases introduced as a function of the temperature. The fact that He gas did not induce a change in the value of ε' is consistent with the previously observed adsorption behavior for **1**.[10]

Figure 4b,c shows the temperature dependence of the real part of relative permittivity for **2** and **3**, respectively, measured under 100 kPa of CO_2, NO, O_2, and He. Changes in the ε' value of compound **2** were similar to those observed for **1**, reflecting their similar adsorption behaviors.[10] The gate-opening transitions $T_{GO\downarrow}$(100 kPa) for **2** were determined to be 242, 155, and 127 K for CO_2, NO, and O_2, respectively (Table 1; ε' for He remained unchanged to 70 K). These gate-opening temperatures for **2** are slightly higher than the corresponding values for **1**, indicating that the [Rh_2]-based framework (packing) in **2** is more flexible than the [Ru_2]-based framework in **1**, even though the compounds are isostructural, which is in good agreement with the results obtained for the sorption isotherms of **1** and **2** at lower pressures (gases begin to be adsorbed by **2** at lower pressures than by **1** at a fixed temperature (Figure S4).[10] On the other hand, as realized from the ε' vs T plots in Figure 4c, compound **3** did not exhibit a decrease in the value of ε'; thus, the gate-opening transition did not occur for any gases used in this study. This result is in complete agreement with the fact that **3** is a nonporous material that is inactive with respect to gas adsorption (Figure S1).

These observations described above indicate that gas adsorption behavior accompanied by gate-opening transitions is detectable with a high degree of accuracy by measuring ac electric field responses as a function of temperature and pressure. Figure 5 shows the temperature dependence of the relative permittivity of **1** measured under several CO_2 pressures during cooling (Figure S5 presents the corresponding data for the heating process). The gate-opening transition was clearly detected as a drastic decrease in the value of ε' at different temperatures and was also found to be strongly dependent on the applied pressure (Table 2). In particular, at pressures below atmospheric pressure, the transition was observed at temperatures less than $T_{GO\downarrow}$(100 kPa). This behavior was similarly observed during heating for the corresponding gate-closing transition (Figure S5), although the transition temperature was observed at higher temperatures and involved thermal

Figure 5. Temperature dependence of the (a) real part (ε') and (b) imaginary part (ε'') of the dielectric constant for **1** measured during cooling under various CO_2 pressures with an ac electric field frequency of 0.1 kHz.

Table 2. Gate-Opening ($T_{GO\downarrow}$) and -Closing ($T_{GO\uparrow}$) Temperatures for 1 under Various Gas Pressures (P) of CO_2 and NO

P (kPa)	$T_{GO\downarrow}$ (K)[a]	$T_{GO\uparrow}$ (K)[a]
@CO_2		
101.4	231	247
49.4	216	235
24.3	203	222
10.7	188	208
4.3	173	196
1.5	162	181
@NO		
100.2	143	161
47.7	133	145
24.1	123	140
9.5	112	130
3.9	102	121
0.4	148	166

[a]$T_{GO\downarrow}$ and $T_{GO\uparrow}$ were defined as the points at which the value was left from and returned to the normal value, respectively.

hysteresis, as mentioned above. The relationship between T_{GO} and the applied P were plotted as $\ln(P)$ vs T^{-1} based on a derivative of the Clausius−Clapeyron equation: $d(\ln(P))/d(T^{-1}) = \Delta H_{Trans}/R_g$, where ΔH_{Trans} is the variation in the transition enthalpy and R_g is the gas constant (Figure 6).[25,26] The plots for the gate-opening and -closing transitions were linear (the P and T^{-1} plots were exponential) and provided transition enthalpy constants (ΔH_{Trans}) for CO_2 of −18.8 and −23.0 kJ mol^{-1}, respectively. Takamizawa et al. have reported a structural phase transition in a similar series of porous chain compounds, $[M_2^{II,II}(PhCO_2)_4(pyz)]$ (M = Rh, Cu; $PhCO_2^-$ = benzoate; pyz = pyrazine), caused by adsorbing CO_2, in which
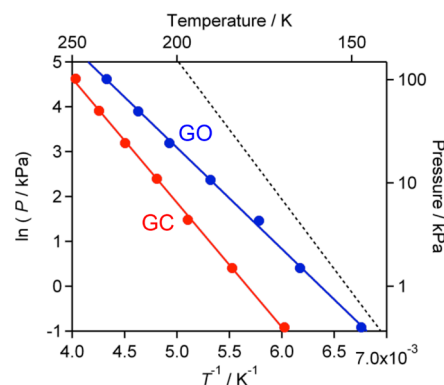
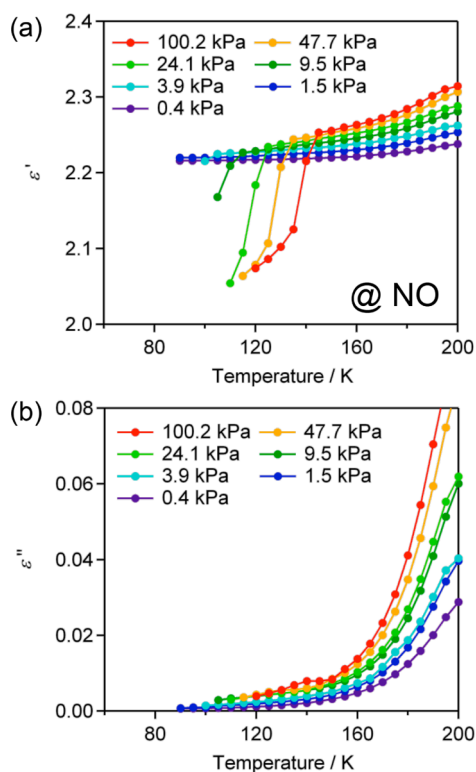Figure 6. Log-scale plots of the CO_2 pressure vs the inverse of the gate-opening (GO; blue) and gate-closing (GC; red) temperatures for **1**. The dashed line represents the freezing point of CO_2 estimated using the Antoine equation ($\log_{10}(P/\text{Torr}) = A - B/\{(T/°C) + C\}$, where $A = 9.81062$, $B = 1347.79$, $C = 272.99$).

ΔH_{Trans} was estimated by *in situ* DSC measurements as −34.5 kJ mol^{-1} (cooling or adsorption) and −39.6 kJ mol^{-1} (heating or desorption) for M = Rh[16a] and −23.5 kJ mol^{-1} (cooling or adsorption) and −33.0 kJ mol^{-1} (heating or desorption) for M = Cu.[16b] Our ΔH_{Trans} values for **1** are smaller than these values, indicating that **1** relatively easily undergoes a structural transition for the CO_2 adsorption. The adsorption enthalpy as an isosteric heat ($q_{st,\Phi=1/e}$) is also possible to be estimated fitting the sorption isotherm based on Dubinin−Radushkevich equation,[28] which derives $q_{st,\Phi=1/e} = 35.7$ kJ mol^{-1} (195 K) based on the evaporative latent heat $\Delta H_v = 25.2$ kJ mol^{-1} for CO_2 (s → g) (Figure S6). However, it should be noted that $q_{st,\Phi=1/e}$ estimated from the DR fitting of isotherms is for the diffusional equilibration in opened pores after the first gate-opening transition, whereas ΔH_{Trans} discussed in this work is originated from the structural transition caused by gas adsorption.

Similar behavior was also observed under an NO atmosphere. The temperature dependence of the permittivity of **1** measured at several NO pressures is shown in Figures 7 (cooling) and S7 (heating), and $T_{GO\downarrow}$ and $T_{GO\uparrow}$ are summarized in Table 2. The $\ln(P)$ vs T^{-1} plots for T_{GO} are depicted in Figure 8. Furthermore, the gate-opening and -closing transitions were closely associated with the temperature and applied pressure, with P and T^{-1} related in an exponential fashion. The transition enthalpy constants for NO were found to be −9.5 kJ mol^{-1} and $\Delta H_{Trans\uparrow} = -14.3$ kJ mol^{-1}, respectively, and were nearly half the corresponding values for CO_2. Thus, based on this relationship for **1**, the gas atmosphere conditions (here, CO_2 and NO) can be readily determined using this technique based on ac electric field responses. Note that an isosteric heat ($q_{st,\Phi=1/e}$) estimated fitting the sorption isotherm for the diffusional equilibration part from after the first gate-opening transition to before the second gate-opening transition based on the DR equation is 23.4 kJ mol^{-1} (121 K) based on the evaporative latent heat $\Delta H_v = 13.8$ kJ mol^{-1} for NO (l → g) (vide supra) (Figure S6).[28]

Specificity for NO Identified in $\varepsilon''-T$ Plots. As briefly mentioned above, ε'' is inversely proportional to resistance R ($\varepsilon'' \propto 1/\omega R$);[27] namely, the temperature dependence of ε'' represents the temperature dependence of the electronic conductivity. It should be emphasized that this electronic behavior is independent of the applied gas pressure if the introduced gas is electronically inert to the host framework. As

Figure 7. Temperature dependence of the (a) real part (ε') and (b) imaginary part (ε'') of the dielectric constant for **1** measured during cooling under various NO pressures with an ac electric field frequency of 0.1 kHz.
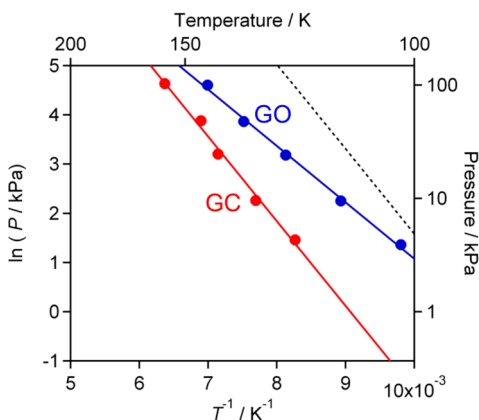
Figure 8. Log-scale plots of the NO pressure vs the inverse of the gate-opening (GO; blue) and gate-closing (GC; red) temperatures for **1**. The dashed line represents the boiling point of NO estimated using the Antoine equation ($\log_{10}(P/\mathrm{Torr}) = A - B/\{(T/°\mathrm{C}) + C\}$, where $A = 8.76685$, $B = 688.314$, and $C = 268.68$).

can be seen in Figure 5, the ε'' vs T plots for **1** obtained under several CO_2 pressures have a similar shape, although the imaginary part of permittivity reflects the change in the ε' value as a small peak anomaly (as characteristically seen in the data at 101.4 kPa in Figure 5). This behavior clearly indicates that CO_2 is electronically inert to the framework of **1**. Meanwhile, the variation in the results for different gases for **1**–**3** seen in Figure 4 was also observed for the ε'' vs T plots for **1** and **3**, which have very similar $[Ru_2]$ frameworks; steep increases in the values for ε'' were observed above 200 K for CO_2, O_2, and He and above 160 K for NO. Because the plots for CO_2, O_2, and

He have an identical shape and these gases are inert for **1** and **3**, it can be concluded that the observed conducting behavior is an inherent aspect of **1** and **3** and/or the samples used; namely, **1** and **3** based on $[Ru_2]$ units are themselves semiconductors. A difference in the ε'' vs T plots for **1** and **3** was only observed for NO. This result clearly indicates that the electronic conductivity of the samples of **1** and **3** was enhanced under an NO atmosphere. This conducting behavior was observed at temperatures above T_{GO} for both **1** and **3**, even though **3** has no pores for gas adsorption. Therefore, this conducting behavior under an NO atmosphere is due to electrical conductivity on the surfaces and through the grain boundaries of the samples. Note that it is very difficult to detect certain types of specific signals (or anomalies) at temperatures below T_{GO} because the compounds remain semiconductors, even under an NO atmosphere. Nevertheless, the specificity for introduced NO of **1** and **3** confirms the existence of host–guest interactions in the pores that enable the selective adsorption of NO for **1**.[10] Host–guest interactions, if they are weak, may vary as a function of the pressure of the guest atmosphere, except for inert gas atmospheres, for which the conductivity would be independent of the pressure as seen for CO_2. The ε'' vs T plots for **1** obtained under several NO pressures (Figures 7 and S7) are different from those obtained under CO_2 (Figures 5 and S5), which reveals a NO pressure dependence of ε''. Namely, this behavior indicates that the electronic conductivity of the sample increases with the pressure of NO. Thus, the ε'' behavior suggests that the specificity for NO stems from NO–$[Ru_2]$ framework interactions.

It is also important to note that such an increase in the value of ε'' was not observed, even with NO, for **2**, which is based on $[Rh_2]$ chains; this indicates that the inherent electronic conductivity of $[Rh_2]$ chains is much lower than that of $[Ru_2]$ chains. This result well explains the difference in the NO adsorption behavior for **1** and **2**.[10]

Impedance Measurements Provide Further Evidence. Investigation of the NO-induced electronic conductivity in detail was then pursed not only to confirm the presence of host–guest interactions during NO-selective adsorption but also to explore the possible application of this system for molecular-induced sensors and electronic devices. The electronic conductivity was evaluated in detail via *in situ* impedance measurements over the frequency range from 10^{-2} to 10^5 Hz using the same sample cell. Semicircles on Nyquist plots were analyzed using a generalized Debye model in the temperature range of 250–350 K (He, CO_2, and O_2) and 180–200 K (NO) for **1** (Figure 9) and **3** (Figure S10) and 420–440 K (He, CO_2, and O_2) for **2** (Figure S9). Figure 9a depicts the Nyquist plots for **1** at 200 K when the respective gases were introduced, together with the plots at 300 K for He, CO_2, and O_2 (inset of Figure 9a) (Figure S9 for **2** and Figure S10 for **3**). Note that impedance measurements under a NO atmosphere were not performed at temperatures above 200 K because the frameworks (or the samples) were gradually eroded when the measurements were repeated. The σ_{ac} values for **1** and **3** with $[Ru_2]$-phz frameworks under He, CO_2, and O_2 were determined to be 10^{-12} to 10^{-13} S cm^{-1} at 300 K (Figure 9b, Table 3) with activation energies of 0.4–0.5 eV (Table 3). In general these values for the conductivity of **1** and **3** are in the range of an insulator but are much higher than that for **2** ($\sigma_{ac} = 10^{-22}$ S cm^{-1} at 300 K (10^{-14} S cm^{-1} at 400 K) with the $[Rh_2]$-phz framework, indicating the conductive nature of the $[Ru_2]$-phz chains. The results at 200 K under He, CO_2, and O_2 were
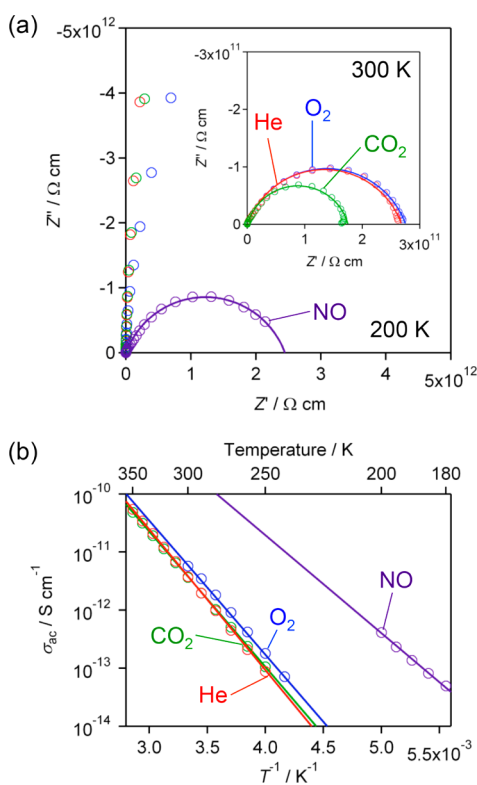
Figure 9. Nyquist plots for **1** at (a) 200 K and (a, inset) 300 K, where the solid lines represent simulated curves based on a generalized Debye equation with β values in the range from 0.74−0.81, and (b) Arrhenius plots of σ_{ac} estimated from the Nyquist plots measured at several temperatures under 100 kPa of He (red), CO_2 (green), O_2 (blue), and NO (violet). The activation energies (E_a) are listed in Table 3.

Table 3. Electronic Conductivities and Activation Energies for 1−3 Evaluated Using the *in Situ* AC Electronic Technique under Various Gas Atmospheres

compounds @ atmosphere	σ_{ac}/S cm^{-1} (200 K)	σ_{ac}/S cm^{-1} (300 K)	σ_{ac}/S cm^{-1} (430 K)	E_a/meV
1@He	3.5×10^{-16a}	3.7×10^{-12}		481
1@CO$_2$	4.9×10^{-16a}	3.6×10^{-12}		462
1@O$_2$	8.4×10^{-16a}	5.7×10^{-12}		459
1@NO	4.1×10^{-13}	2.6×10^{-10a}		335
2@He		3.5×10^{-22a}	8.5×10^{-14}	1.67×10^3
2@CO$_2$		3.1×10^{-21a}	2.9×10^{-14}	1.29×10^3
2@O$_2$		3.2×10^{-20a}	2.9×10^{-14}	1.17×10^3
3@He	6.2×10^{-16a}	7.7×10^{-13}		371
3@CO$_2$	4.1×10^{-16a}	6.8×10^{-13}		386
3@O$_2$	4.1×10^{-16a}	8.5×10^{-13}		398
3@NO	8.5×10^{-14}	8.6×10^{-12a}		239

^{a}Estimated value from the Arrhenius plots.

out of the range of the apparatus used. Meanwhile, the σ_{ac} values for **1** and **3** at 200 K under a NO atmosphere were significant at ~10^{-13} S cm^{-1}, with activation energy of 0.2−0.3 eV (Figure 9a,b, Table 3). The approximated σ_{ac} values for **1** and **3** at 200 K under He, CO_2, and O_2 atmospheres obtained from the Arrhenius plots fell in the 10^{-16} S cm^{-1} range. Therefore, it can be concluded that the NO gas enhanced the conductivity at the grain boundaries by a factor of 10^3. This

conclusion is in good agreement with the ε'' behavior under a NO atmosphere.

■ CONCLUSION

The gate-opening-type adsorption properties and the adsorption selectivity for NO of the porous chain compounds [M_2(4-Cl-2-OMePhCO$_2$)$_4$(phz)] (M = Ru, **1**; Rh, **2**) were electrically monitored by measuring the changes in permittivity and impedance values as a function of temperature after the application of ac electric fields. The required sample was just ~5 mg, and the electric response was rapidly obtained. A sudden decrease in the ε' portion of permittivity was clearly observed when the introduction of gases resulted in opening of the micropores' gates. As expected, such behavior was not observed in the nonporous gate-inactive compound [Ru$_2$(o-OMePhCO$_2$)$_4$(phz)] (**3**). The sensitivity of the gate-opening behavior (in terms of the ΔH_{Trans} value) to the type of gas and two external stimuli (temperature and pressure) follows the Clausius−Clapeyron equation. It should be mentioned that the change in permittivity occurred rapidly over a narrow temperature range, suggesting that the gate-opening transition also occurred rapidly; the variation feature of ε' as a function of temperature could be associated with the dynamics of gate opening. Thus, with this technique, it is possible to roughly know the dynamic behavior of gate-opening/closing phenomena for gas adsorption/desorption in a material, for example, from the temperature-dependent feature of the permittivity anomaly and its temperature range. In other words, these results suggest that it is possible to accurately control the permittivity signals using a known gas pressure. In addition, it was found that the imaginary part (ε'') of permittivity is associated with the conductance; changes in the ε'' value, which can be detected with high sensitivity, reflect the electronic perturbations of sample surfaces and/or framework compositions following the introduction of a gas. Of course, inert gases (He, O_2, and CO_2 in this work) do not cause any significant electronic perturbations, and thus any observed leakage current behavior is attributable to the intrinsic electronic properties of the sample. For compounds **1** and **3** possessing [Ru$_2$]-phz chains, only the introduction of NO led to changers in the ε'' value; the conductivity under an NO atmosphere was clearly much higher than that when the inert gases were introduced. In addition, the conductivity was dependent on the NO gas pressure and was even observed at temperatures greater than T_{GO}, indicating that the NO gas significantly influenced the conductivity through grain boundaries in the sample, i.e., at the sample surface where host−guest electronic interactions are affected by the NO gas pressure. These results well-explain the selective adsorption of NO by **1**.[10]

The measurement of impedance is a highly sensitive analytical technique for investigating the electronic state of materials. Therefore, this technique is quite useful for confirming the presence of electronic host−guest interactions in conducting host frameworks derived from redox-active MOFs. As a result, the specific electronic effects under an NO atmosphere were clearly monitored.

The present observations offer useful information not only about the adsorption behavior and related chemistry of MOFs/PCPs that have recently attracted significant attention but also demonstrate the effectiveness of this new technique for understanding the impact of porous properties on adsorption behavior and provide further support for the possible application of MOFs as chemically driven electronic devices.

Furthermore, based on the results of this study, it can be concluded that MOFs constructed from redox-active building blocks are attractive candidate materials for such applications.

EXPERIMENTAL SECTION

General Procedures and Materials. All synthetic procedures were performed under an inert atmosphere using standard Schlenk-line techniques and a commercial glovebox. All chemicals were purchased from commercial sources and were of reagent-grade quality. Solvents were distilled under a N_2 atmosphere using common drying agents. Compounds **1** and **2** were prepared using a previously reported method.[10]

Preparation of [Ru₂(o-OMePhCO₂)₄(THF)₂].[29] $[Ru_2^{II,III}(CH_3CO_2)_4Cl]$[30] (1.42 g, 3.0 mmol) and *o*-methoxybenzoic acid (1.82 g, 12.0 mmol) were refluxed in MeOH (150 mL) for 48 h. After cooling to room temperature, Zn powder (392 mg, 6.0 mmol) was added to the solution, and the mixture was refluxed for 24 h. Next the solvent was removed via hot filtration, and the brown residue was dried *in vacuo*. The residue was then dissolved in THF (100 mL) and refluxed for 24 h. The resulting brown solution was filtered and layered with *n*-hexane to obtain brown needle crystals after a week (yield: 80%). Elemental analysis (%) calcd. for $C_{40}H_{44}O_{14}Ru_2$: C 50.52, H 4.66. Found: C 50.44, H 4.60. IR (KBr): $\nu(CO_2)$, 1546, 1394 cm^{-1}.

Preparation of 3. A solution of $[Ru_2(o\text{-OMePhCO}_2)_4(THF)_2]$ (38 mg, 0.04 mmol) in CH_2Cl_2 (10 mL) was separated into five portions and placed in narrow-diameter glass tubes (ϕ 8 mm) (bottom layer). A mixed CH_2Cl_2/benzene solvent (1:1 v/v; 1 mL) was placed on top of the first solution in each tube to slow the rate of diffusion (middle layer). Finally, a solution (2 mL) of phz (28 mg, 0.16 mmol) in benzene (10 mL) was carefully placed on the middle layer in each tube (top layer). The glass tubes were left undisturbed for 1 week, after which needle-like brown crystals of **3** were obtained (yield 54%). Elemental analysis (%) calcd. for $C_{44}H_{36}O_{12}Ru_2$: C 53.55, N 2.74, H 3.68. Found: C 53.43, N 2.65, H 3.65. IR (KBr): $\nu(CO_2)$, 1545, 1379 cm^{-1}.

Physical Measurements. Infrared (IR) spectra were recorded for KBr pellets using a HORIBA FT-720 spectrometer. Magnetic susceptibility measurements were conducted using a Quantum Design SQUID magnetometer MPMS-XL on polycrystalline samples in the range of 1.8–300 K at 1000 Oe. The data were corrected for the diamagnetic contribution of the sample using Pascal's constants.[31]

Gas Sorption Measurements. The sorption isotherm measurements for N_2 (at 77 K), O_2 (at 90 K), NO (at 121 K), and CO_2 (at 195 K) were performed using an automatic volumetric adsorption apparatus (BELSORP max; BEL Inc.) connected to a cryostat system. A known weight (ca. 100 mg) of a dried sample was placed into the sample cell, and prior to the analysis, the cell was evacuated for 5 h at 353 K using the degas a function of the analyzer. The change in the pressure was then monitored, and the degree of adsorption was determined based on the decrease in the pressure at the equilibrium state.

***In situ* AC Electric Field Response Measurements.** Dielectric constants in the 0.1–10 kHz frequency range were measured using an Andeen–Hagerling 2700A capacitance bridge with input voltage amplitude ranging from 0.2 to 15 V (the suitable voltage was automatically selected by the instrument). Impedance measurements were performed over the frequency range from 10 mHz to 100 kHz with Solartron SI 1260 impedance and gain-phase analyzer and a Solartron 1296 dielectric interface with a 1 V input voltage amplitude. A powder sample (~5 mg) was compressed into a pellet with a diameter of 10 mm and a thickness of ~0.1 mm and placed between two stainless plates to create a parallel-plate capacitor, to which Au wires were attached using Au paste. The capacitor was then placed in a cryostat system equipped with coaxial cables for dielectric measurement and connected to a gas handling and pressure monitoring system. Prior to performing the analysis, the sample was dried under high vacuum ($<10^{-2}$ Pa) at 353 K for 5 h.

X-ray Crystallographic analysis of 3. Crystal data for **3** were collected at 123 K on a CCD diffractometer (Rigaku Mercury 70) with graphite monochromated Mo-Kα radiation ($\lambda = 0.71070$ Å). A single crystal was mounted on a thin Kapton film using Nujol and cooled in a N_2 gas stream. The structures were solved using direct methods (SIR92),[32] which were expanded using Fourier techniques. The full-matrix least-squares refinement on F^2 was performed based on the observed reflections and variable parameters, and the refinement cycle was estimated from unweighted and weighted agreement factors for $R1 = \sum\|F_0| - |F_c\|/\sum|F_0|$ ($I > 2.00\sigma(I)$ and all data) and $wR2 = [\sum(w(F_0^2 - F_c^2)^2)/\sum w(F_0^2)^2]^{1/2}$ (all data). A Sheldrick weighting scheme was used. Neutral atom scattering factors were taken from Cromer and Waber.[33] Anomalous dispersion effects were included in F_c;[34] the values of $\Delta f'$ and $\Delta f''$ were those of Creagh and McAuley.[35] The values for the mass attenuation coefficients are those of Creagh and Hubbell.[36] All calculations were performed using the Crystal-Structure crystallographic software package,[37] except for refinement, which was performed using SHELXL-97.[38] These data have been deposited as CIFs at the Cambridge Data Centre as supplementary publication no. CCDC-1003673. Copies of the data can be obtained free of charge upon application to CCDC, 12 Union Road, Cambridge CB21EZ, UK (fax: (+44) 1223–336–033; email: deposit@ccdc.ca-m.ac.uk). Structural diagrams were prepared using VESTA software.[39] The void volumes of the crystal structures were estimated using PLATON.[24]

Crystallographic Data for 3. Formula: $C_{44}H_{36}N_2O_{12}Ru_2$, $M_r = 986.91$, Triclinic, $P-1$ (#2), $a = 9.461(3)$ Å, $b = 10.660(4)$ Å, $c = 10.261(4)$ Å, $\alpha = 92.650(4)°$, $\beta = 102.491(5)°$, $\gamma = 96.611(5)°$, $V = 1000.9(6)$ Å^3, $T = 123(1)$ K, $Z = 1$, $D_{calc} = 1.637$ g cm^{-3}, $F_{000} = 498.00$, $\lambda = 0.71070$ Å, μ(Mo-Kα) = 8.232 cm^{-1}, 10994 measured reflections, 4474 unique ($R_{int} = 0.0625$). $R_1 = 0.0532$ ($I > 2\sigma(I)$), $R_1 = 0.0697$ (all data), and $wR_2 = 0.1123$ with GOF = 1.092. CCDC-1003673.

ASSOCIATED CONTENT

Ⓢ Supporting Information

CIF format X-ray crystallographic data, the gas adsorption isotherms, and the magnetic properties for **3**, temperature dependence of the dielectric constant for **1**–**3** under 100 kPa of various gases measured during heating, sorption isotherms for **1** and **2**, temperature dependence of the dielectric constant under various pressure of CO_2 and NO for **1** measured during heating, Nyquist and Arrhenius plots for **2** and **3**. This material is available free of charge via the Internet at http://pubs.acs.org.

AUTHOR INFORMATION

Corresponding Author

miyasaka@imr.tohoku.ac.jp

Notes

The authors declare no competing financial interest.

ACKNOWLEDGMENTS

REFERENCES

(1) (a) Kitagawa, S.; Kitaura, R.; Noro, S. *Angew. Chem., Int. Ed.* **2004**, *43*, 2334–2375. (b) Horike, S.; Shimomura, S.; Kitagawa, S. *Nat. Chem.* **2009**, *1*, 695–704.

(2) (a) Yaghi, O. M.; ÓKeeffe, M.; Ockwig, N. W.; Chae, H. K.; Eddaoudi, M.; Kim, H. *Nature* **2003**, *423*, 705–714. (b) Férey, G. *Chem. Soc. Rev.* **2008**, *37*, 191–214.

(3) Li, J.-R.; Sculley, J.; Zhou, H.-C. *Chem. Rev.* **2012**, *112*, 869–932.

(4) (a) Yang, S.; Sun, J.; Ramirez-Cuesta, A. J.; Callear, S. K.; David, W. I. F.; Anderson, D. P.; Newby, R.; Blake, A. J.; Parker, J. E.; Tang,

C. C.; Schröder, M. *Nat. Chem.* **2012**, *4*, 887–894. (b) Southon, P. D.; Price, D. J.; Nielsen, P. K.; Mckenzie, C. J.; Kepert, C. J. *J. Am. Chem. Soc.* **2011**, *133*, 10885–10891. (c) Sato, H.; Matsuda, R.; Sugimoto, K.; Takata, M.; Kitagawa, S. *Nat. Mater.* **2010**, *9*, 661–666. (d) Vaidhyanathan, R.; Iremonger, S. S.; Dawson, K. W.; Shimizu, G. K. H. *Chem. Commun.* **2009**, 5230–5232. (e) Britt, D.; Tranchemontagne, D.; Yaghi, O. M. *Proc. Natl. Acad. Sci. U. S. A.* **2008**, *105*, 11623–11627. (f) Matsuda, R.; Kitaura, R.; Kitagawa, S.; Kubota, Y.; Belosludov, R. V.; Kobayashi, T. C.; Sakamoto, H.; Chiba, T.; Takata, M.; Kawazoe, Y.; Mita, Y. *Nature* **2005**, *436*, 238–241.

(5) (a) Sato, H.; Kosaka, W.; Matsuda, R.; Hori, A.; Hijikata, Y.; Belosludov, R. V.; Sakaki, S.; Takata, M.; Kitagawa, S. *Science* **2014**, *343*, 167–170. (b) Shimomura, S.; Higuchi, M.; Matsuda, R.; Yoneda, K.; Hijikata, Y.; Kubota, Y.; Mita, Y.; Kim, J.; Takata, M.; Kitagawa, S. *Nat. Chem.* **2010**, *2*, 633–637. (c) Xiao, B.; Byrne, P. J.; Wheatley, P. S.; Wragg, D. S.; Zhao, X.; Fletcher, A. J.; Thomas, K. M.; Peters, L.; Evans, J. S. O.; Warren, J. E.; Zhou, W.; Morris, R. E. *Nat. Chem.* **2009**, *1*, 289–294.

(6) Lin, L.-C.; Kim, J.; Kong, X.; Scott, E.; McDonald, T. M.; Long, J. R.; Reimer, J. A.; Smit, B. *Angew. Chem., Int. Ed.* **2013**, *52*, 4410–4413.

(7) Noro, S.; Tanaka, D.; Sakamoto, H.; Shimomura, S.; Kitagawa, S.; Takeda, S.; Uemura, K.; Kita, H.; Akutagawa, T.; Nakamura, T. *Chem. Mater.* **2009**, *21*, 3346–3355.

(8) (a) Moudrakovski, I. L.; Terskikh, V. V.; Ratcliffe, C. I.; Ripmeester, J. A.; Wang, L.-Q.; Shin, Y.; Exarhos, G. J. *J. Phys. Chem. B* **2002**, *106*, 5938–5946. (b) Huang, S.-J.; Huang, C.-H.; Chen, W.-H.; Sun, X.; Zeng, X.; Lee, H.-K.; Ripmeester, J. A.; Mou, C.-Y.; Liu, S.-B. *J. Phys. Chem. B* **2005**, *109*, 681–684. (c) Pawsey, S.; Moudrakovski, I.; Ripmeester, J.; Wang, L.-Q.; Exarhos, G. J.; Rowsell, J. L. C.; Yaghi, O. M. *J. Phys. Chem. C* **2007**, *111*, 6060–6067. (d) Ueda, T.; Kurokawa, K.; Eguchi, T.; Kachi-Terajima, C.; Takamizawa, S. *J. Phys. Chem. C* **2007**, *111*, 1524–1534. (e) Chandler, B. D.; Enright, G. D.; Udachin, K. A.; Pawsey, S.; Ripmeester, J. A.; Cramb, D. T.; Shimizu, G. K. H. *Nat. Mater.* **2008**, *7*, 229–235. (f) Anedda, R.; Soldatov, D. V.; Moudrakovski, I. L.; Casu, M.; Ripmeester, J. A. *Chem. Mater.* **2008**, *20*, 2908–2920. (g) Comotti, A.; Bracco, S.; Sozzani, P.; Horike, S.; Matsuda, R.; Chen, J.; Takata, M.; Kubota, Y.; Kitagawa, S. *J. Am. Chem. Soc.* **2008**, *130*, 13664–13672. (h) Springuel-Huet, M.-A.; Nossov, A.; Adem, Z.; Guenneau, F.; Volkringer, C.; Loiseau, T.; Férey, G.; Gédéon, A. *J. Am. Chem. Soc.* **2010**, *132*, 11599–11607.

(9) (a) Vimont, A.; Goupil, J.-M.; Lavalley, J.-C.; Daturi, M.; Surblé, S.; Serre, C.; Millange, F.; Férey, G.; Audebrand, N. *J. Am. Chem. Soc.* **2006**, *128*, 3218–3227. (b) Vimont, A.; Travert, A.; Bazin, P.; Lavalley, J.-C.; Daturi, M.; Serre, C.; Férey, G.; Bourrelly, S.; Llewellyn, P. L. *Chem. Commun.* **2007**, 3291–3293. (c) Vimont, A.; Leclerc, H.; Maugé, F.; Daturi, M.; Lavalley, J.-C.; Surblé, S.; Serre, C.; Férey, G. *J. Phys. Chem. C* **2007**, *111*, 383–388. (d) Xiao, B.; Wheatley, P. S.; Zhao, X.; Fletcher, A. J.; Fox, S.; Rossi, A. G.; Megson, I. L.; Bordiga, S.; Regli, L.; Thomas, K. M.; Morris, R. E. *J. Am. Chem. Soc.* **2007**, *129*, 1203–1209. (e) Miller, S. R.; Pearce, G. M.; Wright, P. A.; Bonino, F.; Chavan, S.; Bordiga, S.; Margiolaki, I.; Guillou, N.; Férey, G.; Bourrelly, S.; Llewellyn, P. L. *J. Am. Chem. Soc.* **2008**, *130*, 15967–15981. (f) Bourrelly, S.; Moulin, B.; Rivera, A.; Maurin, G.; Devautour-Vinot, S.; Serre, C.; Devic, T.; Horcajada, P.; Vimont, A.; Clet, G.; Daturi, M.; Lavalley, J.-C.; Loera-Serna, S.; Denoyel, R.; Llewellyn, P. L.; Férey, G. *J. Am. Chem. Soc.* **2010**, *132*, 9488–9498. (g) Murray, L. J.; Dinca, M.; Yano, J.; Chavan, S.; Bordiga, S.; Brown, C. M.; Long, J. R. *J. Am. Chem. Soc.* **2010**, *132*, 7856–7857. (h) Sumida, K.; Brown, C. M.; Herm, Z. R.; Chavan, S.; Bordiga, S.; Long, J. R. *Chem. Commun.* **2011**, *47*, 1157–1159. (i) Leclerc, H.; Vimont, A.; Lavalley, J.-C.; Daturi, M.; Wiersum, A. D.; Llwellyn, P. L.; Horcajada, P.; Férey, G.; Serre, C. *Phys. Chem. Chem. Phys.* **2011**, *13*, 11748–11756. (j) Hamon, L.; Leclerc, H.; Ghoufi, A.; Oliviero, L.; Travert, A.; Lavalley, J.-C.; Devic, T.; Serre, C.; Férey, G.; De Weireld, G.; Vimont, A.; Maurin, G. *J. Phys. Chem. C* **2011**, *115*, 2047–2056. (k) Higuchi, M.; Nakamura, K.; Horike, S.; Hijikata, Y.; Yanai, N.; Fukushima, T.; Kim, Y.; Kato, K.; Takata, M.; Watanabe, D.; Ohima, S.; Kitagawa, S. *Angew. Chem., Int. Ed.* **2012**, *124*, 8494–8497. (l) Wuttke, S.; Bazin, P.; Vimont, A.; Serre, C.; Seo, Y.-K.; Hwang, Y. K.; Chang, J.-S.; Férey, G.; Daturi, M.

Chem.—Eur. J. **2012**, *18*, 11959–11967. (m) Yang, W.; Davies, A. J.; Ling, X.; Suyetin, M.; Matsuda, R.; Blake, A. J.; Wilson, C.; Lewis, W.; Parker, J. E.; Tang, C. C.; George, M. W.; Hubberstey, P.; Kitagawa, S.; Sakamoto, H.; Bichoutskaia, E.; Champness, N. R.; Yang, S.; Schröder, M. *Chem. Sci.* **2012**, *3*, 2993–2999. (n) Devic, T.; Salles, F.; Bourrelly, S.; Moulin, B.; Maurin, G.; Horcajada, P.; Serre, C.; Vimont, A.; Lavalley, J.-C.; Leclerc, H.; Clet, G.; Daturi, M.; Llewellyn, P. L.; Filinchuk, Y.; Férey, G. *J. Mater. Chem.* **2012**, *22*, 10266–10273. (o) Volkringer, C.; Leclerc, H.; Lavalley, J.-C.; Loiseau, T.; Férey, G.; Daturi, M.; Vimont, A. *J. Phys. Chem. C* **2012**, *116*, 5710–5719. (p) Sumida, K.; Stück, D.; Mino, L.; Chai, J.-D.; Bloch, E. D.; Zavorotynska, O.; Murray, L. J.; Dincă, M.; Chavan, S.; Bordiga, S.; Gead-Gordon, M.; Long, J. R. *J. Am. Chem. Soc.* **2013**, *135*, 1083–1091. (q) Yang, S.; Liu, L.; Sun, J.; Thomas, K. M.; Davies, A. J.; George, M. W.; Blake, A. J.; Hill, A. H.; Fitch, A. N.; Tang, C. C.; Schröder, M. *J. Am. Chem. Soc.* **2013**, *135*, 4954–4957.

(10) Kosaka, W.; Yamagishi, K.; Hori, A.; Sato, H.; Matsuda, R.; Kitagawa, S.; Takata, M.; Miyasaka, H. *J. Am. Chem. Soc.* **2013**, *135*, 18469–18480.

(11) (a) Centrone, A.; Siberio-Pérez, D. Y.; Millward, A. R.; Yaghi, O. M.; Matzger, A. J.; Zerbi, G. *Chem. Phys. Lett.* **2005**, *411*, 516–519. (b) Siberio-Pérez, D. Y.; Wong-Foy, A. G.; Yaghi, O. M.; Matzger, A. J. *Chem. Mater.* **2007**, *19*, 3681–3685. (c) Seo, J.; Bonneau, C.; Matsuda, R.; Takata, M.; Kitagawa, S. *J. Am. Chem. Soc.* **2011**, *133*, 9005–9013. (d) Leclerc, H.; Devic, T.; Devautour-Vinot, S.; Bazin, P.; Audebrand, N.; Férey, G.; Daturi, M.; Vimont, A.; Clet, G. *J. Phys. Chem. C* **2011**, *115*, 19828–19840.

(12) (a) Yanai, N.; Kitayama, K.; Hijikata, Y.; Sato, H.; Matsuda, R.; Kubota, Y.; Takata, M.; Mizuno, M.; Uemura, T.; Kitagawa, S. *Nat. Mater.* **2011**, *10*, 787–793. (b) Sokotowski, K.; Bury, W.; Justyniak, I.; Fairen-Jimez, D.; Soltys, K.; Prochowicz, D.; Yang, S.; Schröder, M.; Lewiński, J. *Angew. Chem., Int. Ed.* **2013**, *52*, 13414–13418.

(13) Lu, G.; Hupp, J. T. *J. Am. Chem. Soc.* **2010**, *132*, 7832–7833.

(14) Gassensmith, J. J.; Kim, J. Y.; Holcroft, J. M.; Farha, O. K.; Stoddart, J. F.; Hupp, J. T.; Jeong, N. K. *J. Am. Chem. Soc.* **2014**, *136*, 8277–8282.

(15) (a) Kitaura, R.; Kitagawa, S.; Kubota, Y.; Kobayashi, T. C.; Kindo, K.; Mita, Y.; Matsuo, A.; Kobayashi, M.; Chang, H.-C.; Ozawa, T. C.; Suzuki, M.; Sakata, M.; Takata, M. *Science* **2002**, *298*, 2358–2361. (b) Takamizawa, S.; Nakata, E.; Akatsuka, T. *Angew. Chem., Int. Ed.* **2006**, *45*, 2216–2221. (c) Takamizawa, S.; Nakata, E.; Akatsuka, T.; Kachi-Terajima, C.; Miyake, R. *J. Am. Chem. Soc.* **2008**, *130*, 17882–17892. (d) Ohba, M.; Yoneda, K.; Agustí, G.; Muñoz, M. C.; Gaspar, A. B.; Real, J. A.; Yamasaki, M.; Ando, H.; Nakao, Y.; Sakaki, S.; Kitagawa, S. *Angew. Chem., Int. Ed.* **2009**, *48*, 4767–4771.

(16) (a) Takamizawa, S.; Nakata, E.; Yokoyama, H.; Mochizuki, K.; Mori, W. *Angew. Chem., Int. Ed.* **2003**, *42*, 4331–4334. (b) Takamizawa, S.; Nakata, E.; Yokoyama, H. *Inorg. Chem. Commun.* **2003**, *6*, 763–765.

(17) (a) Rowsell, J. L. C.; Eckert, J.; Yaghi, O. M. *J. Am. Chem. Soc.* **2005**, *127*, 14904–14910. (b) Brown, C. M.; Liu, Y.; Yildirim, T.; Peterson, V. K.; Kepert, C. J. *Nanotechnology* **2009**, *20*, 204025. (c) Sumida, K.; Horike, S.; Kaye, S. S.; Herm, Z. R.; Queen, W. L.; Brown, C. M.; Grandjean, F.; Long, G. J.; Dailly, A.; Long, J. R. *Chem. Sci.* **2010**, *1*, 184–191. (d) Queen, W. L.; Bloch, E. D.; Brown, C. M.; Hudson, M. R.; Mason, J. A.; Murray, L. J.; Ramirez-Cuesta, A. J.; Peterson, V. K.; Long, J. R. *Dalton Trans.* **2012**, *41*, 4180–4187. (e) Lalonde, M. B.; Getman, R. B.; Lee, J. Y.; Roberts, J. M.; Sarjeant, A. A.; Scheidt, K. A.; Georgiev, P. A.; Embs, J. P.; Eckert, J.; Farha, O. K.; Snurr, R. Q.; Hupp, J. T. *CrystEngComm* **2013**, *15*, 9408–9414. (f) Tranchemontagne, D. J.; Park, K. S.; Furukawa, H.; Eckert, J.; Knobler, C. B.; Yaghi, O. M. *J. Phys. Chem. C* **2012**, *116*, 13143–13151.

(18) (a) Peterson, V. K.; Liu, Y.; Brown, C. M.; Kepert, C. J. *J. Am. Chem. Soc.* **2006**, *128*, 15578–15579. (b) Lin, X.; Telepeni, I.; Blake, A. J.; Dailly, A.; Brown, C. M.; Simmons, J. M.; Zoppi, M.; Walker, G. S.; Thomas, K. M.; Mays, T. J.; Hubberstey, P.; Champness, N. R.; Schröder, M. *J. Am. Chem. Soc.* **2009**, *131*, 2159–2171. (c) Peterson,

V. K.; Brown, C. M.; Liu, Y.; Kepert, C. J. *J. Phys. Chem. C* **2011**, *115*, 8851−8857.

(19) Drisdell, W. S.; Poloni, R.; McDonald, T. M.; Long, J. R.; Smit, B.; Neaton, J. B.; Prendergast, D.; Kortright, J. B. *J. Am. Chem. Soc.* **2013**, *135*, 18183−18190.

(20) (a) Mellot-Draznieks, C.; Serre, C.; Surblé, S.; Audebrand, N.; Férey, G. *J. Am. Chem. Soc.* **2005**, *127*, 16273−16278. (b) Kitaura, R.; Matsuda, R.; Kubota, Y.; Kitagawa, S.; Takata, M.; Kobayashi, T. C.; Suzuki, M. *J. Phys. Chem. B* **2005**, *109*, 23378−23385. (c) Llewellyn, P. L.; Bourrelly, S.; Serre, C.; Filinchuk, Y.; Férey, G. *Angew. Chem., Int. Ed.* **2006**, *45*, 7751−7754. (d) Kubota, Y.; Takata, M.; Matsuda, R.; Kitaura, R.; Kitagawa, S.; Kobayashi, T. C. *Angew. Chem., Int. Ed.* **2006**, *45*, 4932−4936. (e) Serre, C.; Bourrelly, S.; Vimont, A.; Ramsahye, N. A.; Maurin, G.; Llewellyn, P. L.; Daturi, M.; Filinchuk, Y.; Leynaud, O.; Barnes, P.; Férey, G. *Adv. Mater.* **2007**, *19*, 2246−2251. (f) Llewellyn, P. L.; Maurin, G.; Devic, T.; Loera-Sema, S.; Rosenbach, N.; Serre, C.; Bourrelly, S.; Horcajada, P.; Filinchuk, Y.; Férey, G. *J. Am. Chem. Soc.* **2008**, *130*, 12808−12814. (g) Navarro, J. A. R.; Barea, E.; Rodríguez-Diéguez, A.; Salas, J. M.; Ania, C. O.; Parra, J. B.; Masciocchi, N.; Galli, S.; Sironi, A. *J. Am. Chem. Soc.* **2008**, *130*, 3978−3984. (h) Hamon, L.; Llewellyn, P. L.; Devic, T.; Ghoufi, A.; Clet, G.; Guillerm, V.; Pirngruber, G. D.; Maurin, G.; Serre, C.; Driver, G.; van Beek, W.; Jolimaître, E.; Vimont, A.; Daturi, M.; Férey, G. *J. Am. Chem. Soc.* **2009**, *131*, 17490−17499. (i) Llewellyn, P. L.; Horcajada, P.; Maurin, G.; Devic, T.; Rosenbach, N.; Bourrelly, S.; Serre, C.; Vincent, D.; Loera-Serna, S.; Filinchuk, Y.; Férey, G. *J. Am. Chem. Soc.* **2009**, *131*, 13002−13008. (j) Seo, J.; Matsuda, R.; Sakamoto, H.; Bonneau, C.; Kitagawa, S. *J. Am. Chem. Soc.* **2009**, *131*, 12792−12800. (k) Matsuda, R.; Kitaura, R.; Kubota, Y.; Kobayashi, T. C.; Takata, M.; Kitagawa, S. *Microporous Mesoporous Mater.* **2010**, *129*, 296−303. (l) Millange, F.; Guillou, N.; Medina, M. E.; Férey, G.; Carlin-Sinclair, A.; Golden, K. M.; Walton, R. I. *Chem. Mater.* **2010**, *22*, 4237−4245. (m) Matsuda, R.; Tsujino, T.; Sato, H.; Kubota, Y.; Morishige, K.; Takata, M.; Kitagawa, S. *Chem. Sci.* **2010**, *1*, 315−321. (n) Zlotea, C.; Campesi, R.; Cuevas, F.; Leroy, E.; Dibandjo, P.; Volkringer, C.; Loiseau, T.; Férey, G.; Latroche, M. *J. Am. Chem. Soc.* **2010**, *132*, 2991−2997. (o) Bureekaew, S.; Sato, H.; Matsuda, R.; Kubota, Y.; Hirose, R.; Kim, J.; Kato, K.; Takata, M.; Kitagawa, S. *Angew. Chem., Int. Ed.* **2010**, *49*, 7660−7664.

(21) (a) Halder, G. J.; Kepert, C. J. *J. Am. Chem. Soc.* **2005**, *127*, 7891−7900. (c) Rowsell, J. L. C.; Spencer, E. C.; Eckert, J.; Howard, J. A. K.; Yaghi, O. M. *Science* **2005**, *309*, 1350−1354.

(22) Miyasaka, H. *Acc. Chem. Res.* **2013**, *46*, 248−257.

(23) Miyasaka, H.; Motokawa, N.; Atsuumi, R.; Kamo, H.; Asai, Y.; Yamashita, M. *Dalton Trans.* **2011**, *40*, 673−682.

(24) Spek, A. L. *Acta Crystallogr., Sect. A* **1990**, *46*, 194−201.

(25) Uemura, K.; Yamasaki, Y.; Komagawa, Y.; Tanaka, K.; Kita, H. *Angew. Chem., Int. Ed.* **2007**, *46*, 6662−6665.

(26) (a) Uemura, K.; Kitagawa, S.; Fukui, K.; Saito, K. *J. Am. Chem. Soc.* **2004**, *126*, 3817−3828. (b) Uemura, K.; Kitagawa, S.; Saito, K.; Fukui, K.; Matsumoto, K. *J. Therm. Anal. Calorim.* **2005**, *81*, 529−532.

(27) Barsoukov, E.; Macdonald, J. R. *Impedance Spectroscopy*; Wiley-interscience: New York, 2005.

(28) Matsuda, R.; Kitaura, R.; Kitagawa, S.; Kubota, Y.; Kobayashi, T. C.; Horike, S.; Takata, M. *J. Am. Chem. Soc.* **2004**, *126*, 14063−14070.

(29) Itoh, M.; Asai, Y.; Kamo, H.; Miura, A.; Miyasaka, H. *Chem. Lett.* **2012**, *41*, 26−28.

(30) Mitchell, R. W.; Spencer, A.; Wilkinson, G. *J. Chem. Soc., Dalton Trans.* **1973**, 846−854.

(31) *Theory and Applications of Molecular Paramagnetism*Boudreaux, E. A., Mulay, L. N., Eds.; John Wiley & Sons: New York, 1976.

(32) Altomare, A.; Cascarano, G.; Giacovazzo, C.; Guagliardi, A.; Burla, M.; Polidori, G.; Camalli, M. *J. Appl. Crystallogr.* **1994**, *27*, 435−441.

(33) Cromer, D. T.; Waber, J. T. *International Tables for Crystallography*; Kynoch Press: Birmingham, England, 1974; Vol. *IV*, Table 2.2A.

(34) Ibers, J. A.; Hamilton, W. C. *Acta Crystallogr.* **1964**, *17*, 781−782.

(35) Creagh, D. C.; McAuley, W. J. *International Tables for Crystallography*; Wilson, A. J. C., Ed.; Kluwer Academic: Boston, MA, 1992; Vol. *C*, Table 4.2.6.8, pp 219−222.

(36) Creagh, D. C.; Hubbell, J. H. *International Tables for Crystallography*; Wilson, A. J. C., Ed.; Kluwer Academic: Boston, MA, 1992; Vol. *C*, Table 4.2.4.3, pp 200−206.

(37) *CrystalStructure 4.0.1: Crystal Structure Analysis Package*; Rigaku Corp.: Tokyo, Japan, 2000−2010; pp 196−8666.

(38) SHELX97: Sheldrick, G. M. *Acta Crystallogr.* **2008**, *A64*, 112−122.

(39) Momma, K.; Izumi, F. *J. Appl. Crystallogr.* **2008**, *41*, 653−658.